Insights from *Operando* and Identical Location (IL) Techniques on the Activation of Electrocatalysts for the Conversion of CO$_2$: A Mini-Review

Abhijit Dutta*[a], Kiran Kiran[a], Motiar Rahaman[a#], Ivan Zelocualtecatl Montiel[a], Pavel Moreno-García[a], Soma Vesztergom[a,b], Jakub Drnec[c], Mehtap Oezaslan[d], and Peter Broekmann*[a]

Abstract: In this mini-review we compare two prototypical metal foam electrocatalysts applied to the transformation of CO$_2$ into value-added products (*e.g.* alcohols on Cu foams and formate on Bi foams). A substantial improvement in the catalyst performance is typically achieved through thermal annealing of the as-deposited foam materials, followed by the electro-reduction of the pre-formed oxidic precursors prior or during the actual CO$_2$ electrolysis. Utilizing highly insightful and sensitive complementary *operando* analytical techniques (XAS, XRD, and Raman spectroscopy) we demonstrate that this catalyst pre-activation process is entirely accomplished in case of the oxidized Cu foams prior to the formation of hydrocarbons and alcohols from the CO$_2$. The actually active catalyst is therefore the metallic Cu derived from the precursor by means of oxide electro-reduction. Conversely, in their oxidic form, the Cu-based foam catalysts are inactive towards the CO$_2$ reduction reaction (denoted ec-CO$_2$RR). Oxidized Bi foams can be regarded as an excellent counter example to the above-mentioned Cu case as both metallic and the thermally derived oxidic Bi foams are highly active towards ec-CO$_2$RR (formate production). Indeed, *operando* Raman spectroscopy reveals that CO$_2$ electrolysis occurs upon its embedment into the oxidic Bi$_2$O$_3$ foam precursor, which itself undergoes partial transformation into an active sub-carbonate phase. The potential-dependent transition of sub-carbonates/oxides into the corresponding metallic Bi foam dictates the characteristic changes of the ec-CO$_2$RR pathway. Identical location (IL) microscopic inspection of the catalyst materials, *e.g.* by means of scanning electron microscopy, demonstrates substantial morphological alterations on the nm length scale on the material surface as consequence of the sub-carbonate formation and the potential-driven oxide reduction into the metallic Bi foam. The foam morphology on a mesoscopic length scale (macroporosity) remains, by contrast, fully unaffected by these phase transitions.

Keywords: Catalyst activation · CO$_2$ reduction reaction · Identical location (IL) technique · Metal foam · *Operando* spectroscopy

Dr. Abhijit Dutta obtained his PhD in chemistry from the Indian Institute of Engineering Science and Technology, Kolkata. During his PhD studies, his research mainly focused on the development of Pt and *non*-Pt based nanostructured materials for the application to fuel cells such as alcohol electro-oxidation, hydrogen oxidation, and the oxygen reduction reaction. He worked as a post-doctoral fellow at the National University of Singapore, Singapore. In 2015 he joined the interfacial electro-chemistry group of Prof. Peter Broekmann at the University of Bern, Switzerland, where he focuses on the development of various *operando* techniques (Raman, XAS, and XRD) to characterize novel electrocatalysts for the selective conversion of CO$_2$ into value-added products.

Kiran Kiran received her MSc in physics from Maharshi Dayanand University (M.D.U.) India in 2015. She is currently pursuing her PhD at the Department of Chemistry, Biochemistry and Pharmaceutical Sciences at the University of Bern under the supervision of Prof. Peter Broekmann. Her research interests are focused on the synthesis of novel electrocatalysts for CO$_2$RR applications.

Dr. Motiar Rahaman received his MSc in chemistry (2013) from the Indian Institute of Technology Madras, India. He obtained his PhD (2018) from the University of Bern (group of Peter Broekmann) on the topic of electrochemical conversion of CO$_2$ into value-added products. Currently he works as a post-doctoral fellow at the University of Cambridge (UK).

Correspondence: Prof. Dr. P. Broekmann[a], E-mail: peter.broekmann@dcb.uni-be.ch; Dr. A. Dutta[a], E-mail: abhijit.dutta@dcb.unibe.ch
[a]University of Bern, Department of Chemistry, Biochemistry and Pharmaceutical Sciences; [b]Eötvös Loránd University, Department of Physical Chemistry, H-1117 Budapest, Pázmány Péter sétány 1/A, Hungary; [c]European Synchrotron Radiation Facility, Grenoble, France; [d]Institute of Technical Chemistry, Technical University of Braunschweig, Braunschweig, Germany; [#]Current address: Department of Chemistry, University of Cambridge, Cambridge, United Kingdom

Ivan Zelocualtecatl Montiel received his BSc and MSc in chemistry from the Meritorious Autonomous University of Puebla (BUAP) in 2013 and 2016, respectively. He is currently a PhD candidate at the Department of Chemistry, Biochemistry and Pharmaceutical Sciences at the University of Bern under the supervision of Prof. Dr. Peter Broekmann. His research interest is focused on the development of novel catalysts for the electroreduction of CO_2.

Dr. Pavel Moreno-García received his PhD in chemistry and molecular science from the University of Bern in 2013, under the supervision of Prof. Dr. Thomas Wandlowski. At that time, his work was devoted to the study of electron transport through nano-objects at electrified interfaces by *in situ* STM. In 2013, he joined the group of Prof. Dr. Peter Broekmann, where he is involved in research activities on electrocatalysis, metal corrosion and laser ablation mass spectrometry.

Dr. Soma Vesztergom obtained his MSc (2010) and PhD (2014) degrees in chemistry, working with Prof. Dr. G. G. Láng at Eötvös Loránd University, Hungary. He was a post-doctoral researcher in Prof. Dr. Peter Broekmann's group at the University of Bern for one year (2014) and is a regular collaborator of this group since then. His research primarily focuses on instrumental developments in electrochemistry and on the modelling of electrocatalytic processes. Currently, he is an assistant professor at Eötvös Loránd University in Budapest.

Dr. Jakub Drnec obtained his PhD degree at University of Victoria, Canada, in the field of surface electrochemistry. He is currently beamline scientist at the European Synchrotron (ESRF) in Grenoble (France), developing new high energy X-rays experimental techniques to study materials for energy conversion and storage. His main goal is to probe materials in their working environment in order to better understand their functioning. His current projects involve *operando* investigations of fuel cells and batteries, fundamental studies of electrocatalyst's degradation and structure-activity relationships, and development of *operando* electrochemical cells and data analysis routines.

Prof. Dr. Mehtap Oezaslan obtained her PhD degree (2012) in electrochemistry from Technische Universität Berlin, Germany. After a post-doctoral stay at the Electrochemistry Laboratory Group, Paul Scherrer Institute, Switzerland, she was a Junior professor for Electrochemistry at Carl von Ossietzky University of Oldenburg from 2014–2019. Since June 2019, she holds a Full (W3) Professorship at the Institute of Technical Chemistry, Technische Universität Braunschweig. Her research is focused on the development and characterization of electrocatalysts for PEM fuel cells and electrolysis.

Prof. Dr. Peter Broekmann obtained his MSc in chemistry (1998) and a PhD (2000) from the University of Bonn. After a post-doctoral stay at the University of Twente (The Netherlands) in 2001, he became project leader at the Institute of Physical Chemistry in Bonn. Since 2008 he holds a lecturer position for electrochemistry at the University of Bern. His research focuses on metal deposition processes for semiconductor and electrocatalysis applications.

1. Introduction

The conversion of CO_2 into value-added products by means of electrolysis (denoted hereafter ec-CO_2RR) is considered a promising approach to mitigate the negative impact that CO_2 is exerting on the global climate.[1] The vision of converting this environmentally harmful molecule into chemical platform chemicals or synthetic fuels on large industrial scale even offers the unique chance of decreasing the existing atmospheric CO_2 concentration, which already exceeds a level of 400 ppm. For this purpose, the ec-CO_2RR has to be coupled in the future to advanced direct air capture technologies.[2–4] The products of CO_2 reduction – typically light-weight molecules such as carbon monoxide, formic acid or alcohols – could be used as either chemical feedstock and transformed further into products of higher value, *e.g.* via Fischer–Tropsch synthesis or biotechnological transformations,[5] or directly as 'green' fuels. The latter is considered vital for the so-called 'energy transition'.[6,7] In particular, if a surplus of renewable energies, originating from solar, wind, or hydroenergy sources, is used to operate the highly endergonic and energy demanding ec-CO_2RR, this conversion process might become truly sustainable and possibly a key element of a future circular economy. Without doubt, ec-CO_2RR has the highest potential of contributing to the closing of the anthropogenic CO_2 cycle (see Fig. 1).[8]
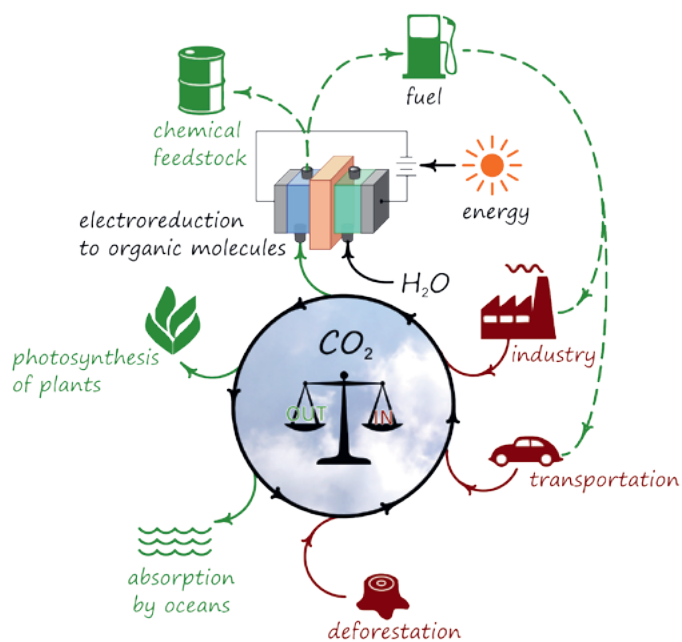

Fig. 1. Schematic depiction of the overall concept to close the anthropogenic carbon cycle by ec-CO_2RR: Towards sustainable conversion of CO_2 into synthetic fuels and chemical feedstock powered by solar energy. Adapted from ref. [8], with permission from John Wiley and Sons.

Most of the known electrochemical CO_2 transformations are, however, still immature and uneconomic.[9] One reason for this is related to electrocatalysts which still require substantial improve-
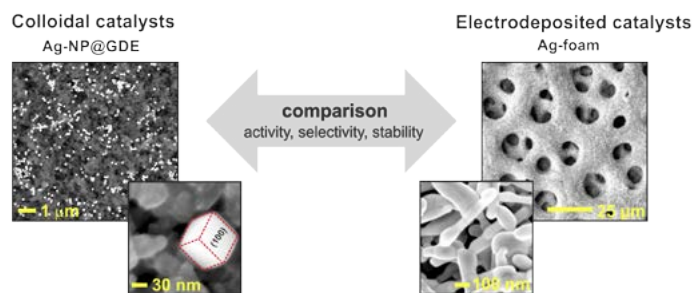
Fig. 2. Complementary catalyst concepts for the ec-CO_2RR: carbon-supported colloidal nanoparticles (left) *versus* electrodeposited metal foams (right) exemplified for Ag-based electrocatalysts. Adapted from refs [13,19], with permission of the American Chemical Society.

ments in terms of material costs, (energy) efficiency and catalyst reliability (stability).[8] Additionally, electrocatalysts are essential not only to accelerate the intrinsically slow ec-CO_2RR process but also to direct the electrolysis reaction towards the desired reaction products (selectivity).[10] It is, however, not only the chemical nature of the catalyst itself which governs the resulting ec-CO_2RR product distribution[10] but also its morphological characteristics on various length scales.[11] Some of the most common ec-CO_2RR catalyst concepts rely on the use of nanoparticulate materials.[12] A clear advantage of this classical approach of catalyst design is that the whole spectrum of (mature) colloid chemistry can be applied to synthesize nano-materials of various shapes, morphologies and size distributions. In addition, this approach offers a straightforward and well-established route to functionalize highly porous carbon supports (*e.g.* gas diffusion electrodes (GDEs), Fig. 2) that are used in gas-fed electrolyzer systems that can reach ec-CO_2RR current densities of technological relevance (> 200 mA × cm^{-2}).[13,14]

A relatively new and alternative concept of ec-CO_2RR catalyst design relies on the electrodeposition of foam-type materials[11,15–17] (Fig. 2), which, similar to their nanoparticulate counterparts, offer a large surface area that is not only accessible to reactants but also enables fast, multidimensional electron transport.[17] Moreover, self-standing foams can directly be employed as cathodes for the ec-CO_2RR often without the need for additional mechanical support, rendering the application of conductive binders unnecessary.[17]

Herein we review and compare the structural, compositional and performance characteristics of two prototypical foam electrocatalysts that are based on Cu and Bi systems published recently.[11,18–20] Among various materials studied so far, Cu stands out as the only known mono-metallic catalyst that can produce multiple hydrocarbons and alcohols of various chain lengths at elevated rates from the ec-CO_2RR.[10,21–26] In this context, C–C

coupled (liquid) alcohols are of particular interest due to their high volumetric energy density (*e.g.* n-propanol: 27.0 MJ L^{-1}).[27] Note that, prior to their use in operating electrolyzers, numerous as-synthesized/as-deposited ec-CO_2RR catalysts require further activation as an essential pre-requisite to attain a highly selective CO_2 conversion into the targeted product(s).[28–33] The terms 'as-synthesized' and 'as-deposited' refer to the stage of catalyst preparation right after the initial electrodeposition of the catalyst material and prior to its further activation. A common approach of such catalyst activation involves the partial or complete surface oxidation of the as-deposited metallic foams, *e.g.* by thermal annealing in air.[20,29,31] An ultimate activation step of such formed oxidic catalyst precursors is often only achieved *in situ* under reductive conditions prior to or during the actual CO_2 electrolysis.[19,31,34] Such oxidation/electro-reduction treatments not only lead to the further increase of the electrochemically active surface area of the catalyst but also often create those active sites on the foam surface which are required for highly selective ec-CO_2RR.[28] It should be emphasized that, at least in the case of copper-based materials, the oxidic precursors (Cu_2O or CuO) formed upon thermal annealing are thermodynamically instable at electrolysis potentials typically applied during ec-CO_2RR,[35] which in turn results into the formation of so-called oxide-derived (OD) catalysts.[31,36] In general, one possible complication of this catalyst activation approach lies in the reduced electric conductivity of the formed 'bulk' oxides. This can, in principle, lead to a 'kinetic' stabilization of the formed oxidic catalyst precursor phases even under the extremely cathodic potentials applied. In some rare cases one might therefore observe oxidic catalyst species even at potentials far beyond the stability regime predicted by thermodynamics. The specific role of oxides for the ec-CO_2RR mechanism and in particular the occurrence of oxygen species embedded inside the hosting metallic Cu matrix under reductive conditions are still the subject of highly controversial debates. To date, there is no ultimate consensus achieved in the literature on the potential-dependent stability of surface and sub-surface oxide/oxygen species and their specific role for the ec-CO_2RR.[19,20,33,37–42] To address these mechanistic questions of catalyst activation, a highly complementary approach utilizing several *operando* techniques is needed, which provides various means of deriving structural and chemical information of the catalyst state under reactive conditions.[28] When further combined with high-resolution imaging techniques, *e.g.* identical-location electron microscopy (*e.g.* IL-SEM[28] or IL-TEM[43]), this holistic approach even permits discriminating *transient* phenomena of catalyst precursor reduction (activation). Fig. 3 depicts the set of complementary *operando* analytical techniques described herein.[19]

X-ray absorption spectroscopy (XAS)[19] provides information on (i) the oxidation state (XANES: X-ray Absorption Near
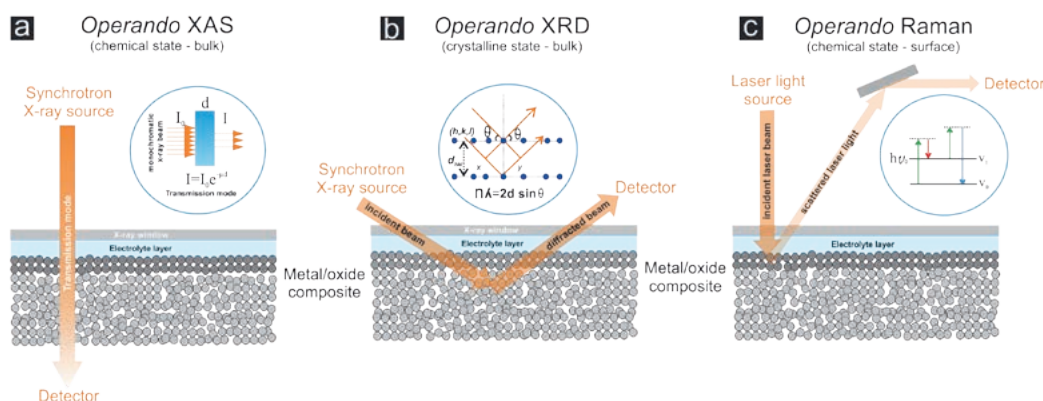

Fig. 3. Complementary *operando* analytical approaches to study the potential-dependent oxide precursor–metal conversion. a) *Operando* X-ray absorption spectroscopy (XAS); b) *Operando* X-ray diffraction (XRD); c) *Operando* Raman spectroscopy. Adapted from ref. [19], with permission of Elsevier.
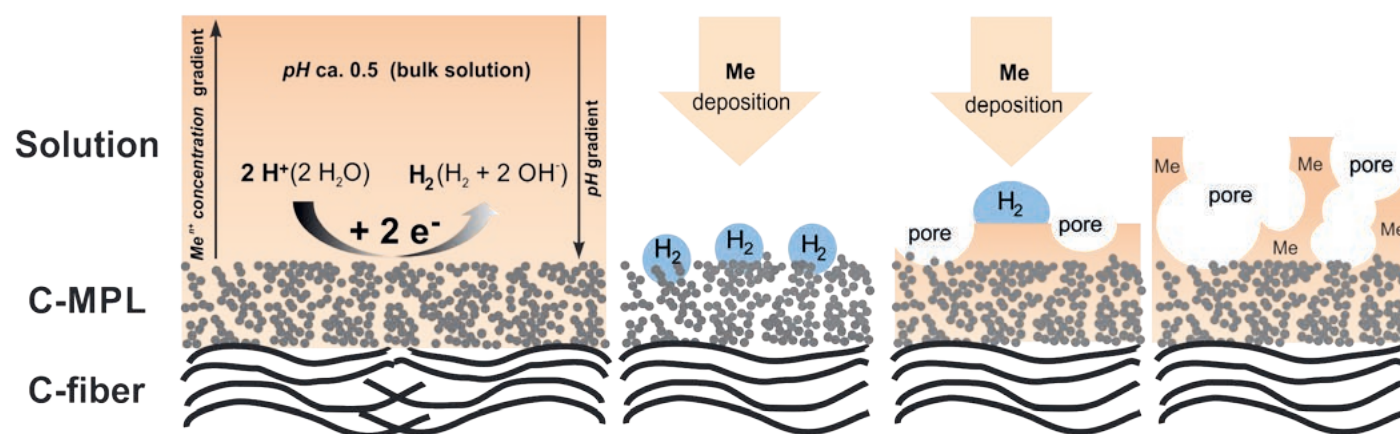
Fig. 4. Metal foam electrodeposition ('Me' deposition) by means of the dynamic hydrogen bubble template (DHBT) approach. The working principle is exemplified for a porous carbon support that finds use as gas-diffusion electrode (GDE). 'MPL' and 'Me' stand for microporous layer and metal, respectively. Adapted from ref. [18], with permission of the American Chemical Society.

Edge Structure) and (ii) the coordination number changes (EXAFS: Extended X-ray Absorption Fine Structure) that typically go along with the electro-reduction of the oxidic precursor materials. Compared to their nanoparticulate counterparts, metal foam electrocatalysts and their oxidic precursors exhibit a more unfavorable surface to volume (bulk) ratio (see *e.g.* Fig. 2). Therefore, information derived from XANES and EXAFS techniques originate predominantly from the 'bulk' of the foam material and comprise only marginal contributions from the respective catalyst surfaces. However, what makes the *operando* grazing-incidence X-ray absorption spectroscopy particularly valuable is its capability to probe these potential-dependent oxidation state transitions even when amorphous phases, lacking any long-range translational order, are involved. Note that the activation of Cu foam catalysts *via* thermal annealing and subsequent electroreduction often proceeds *via* amorphous Cu_xO phases.[19,20]

The *operando* X-ray diffraction (XRD) technique[19] is highly complementary to XAS as it permits probing changes in the crystal structure of the foam catalysts, which typically accompany the potential-driven oxidation state changes.

Raman spectroscopy[19] can be considered as the most surface sensitive *operando* technique among those employed herein. A particular strength of the *operando* Raman spectroscopy is that not only the potential-induced alterations of the catalyst themselves can be probed but, in addition, also the emergence of ec-CO_2RR intermediate species, which might be chemisorbed on the evolving 'active' metallic catalyst surface.[19,44]

Herein we introduce Cu foams and their oxidic precursors as prototypical model systems where the oxide–metal transition (catalyst activation) is completed prior to (or at the very onset of) the ec-CO_2RR.[19,20,28] The actual foam catalysts, being active towards alcohol and hydrocarbons, can therefore be considered as truly oxide-derived (OD).[19]

As a counter-example to that, we also discuss oxidized Bi foam catalysts[18] used for the highly selective production of formate. Our investigations reveal that both the oxidized as well as the corresponding metallic foams exhibit pronounced electrocatalytic activity towards the ec-CO_2RR. Finally, we hint at two ec-CO_2RR pathways that are distinctly active on oxide-derived Cu and Bi_2O_3/Bi foam electrocatalysts.[18]

2. Experimental[18,19]

Experimental details on the Cu and Bi foam preparation and the performed *operando*/IL investigations have already been detailed elsewhere.[11,18,19] We therefore restrict ourselves here to a brief description of the applied experimental approaches.

2.1 Preparation of the Cu/Cu$_x$O and Bi/Bi$_2$O$_3$ Foam Catalysts[11,19]

Metallic Cu foams were electrodeposited onto activated carbon foil substrates (0.25 mm thick, 99.8%, Alfa Aesar, Germany) using the dynamic hydrogen bubble template (DHBT)[15,16] approach (see Fig. 4). The carbon foil support was then immersed into a Cu plating bath containing 0.2 M $CuSO_4 \cdot 5H_2O$ and 1.5 M H_2SO_4. For the galvanostatic deposition process, a current density of $j = -3.0 \text{ A} \times \text{cm}^{-2}$ (normalized to the geometric surface area of the carbon support) was applied for the duration of 5 seconds. The electrodeposited Cu foams were further subjected to thermal annealing in air for 12 h at a temperature of 300 °C using a tube furnace (GERO, GmbH, Germany).

For the *operando* Raman spectroscopy studies, metallic Bi foams were electrodeposited on graphitic carbon foils (Alfa Aesar) that were activated prior to the Bi deposition by annealing in air at 550 °C for 12 h in a tube furnace. To further increase the electrochemically active surface area Bi foams were deposited on highly porous carbon fiber cloths (gas diffusion electrodes, GDEs, Fuel Cell, USA) for the electrolysis experiments. The carbon fiber cloths were used as received. The standard plating bath for the Bi foam deposition was composed of 1.5 M H_2SO_4 (prepared from 96% H_2SO_4, ACS grade, Sigma-Aldrich) serving as the supporting electrolyte and 20 mM bismuth ammonium citrate ($C_{12}H_{22}BiN_3O_{14}$, purity ≥ 99.5 % Sigma Aldrich). The galvanostatic Bi foam deposition was carried by applying a current density of $j = -3.0 \text{ A} \times \text{cm}^{-2}$ (referred to the geometric surface area of the support electrode) for 20 s. The as-prepared Bi foams were further subjected to thermal annealing in air at 300 °C for 12 h, thus transforming the metallic Bi into fully oxidized Bi_2O_3.

2.2 Operando X-ray Absorption Spectroscopy[19]

XAS experiments were carried out at the SuperXAS (X10DA) beamline at the Swiss Light Source (SLS) in Villigen, Switzerland. The storage ring was operated at 2.4 GeV and 400 mA. For the *operando* spectroscopic experiments a dedicated liquid flow-cell was used.[45] XAS experiments were carried out in CO_2-sat. 0.5 M $KHCO_3$ electrolyte solution (pH = 7.2) in the potential range from +0.8 V to –0.9 V vs. RHE. All potentials were iR-corrected.

2.3 Operando X-ray Diffraction[19]

Operando XRD experiments were performed at the high energy beamline ID31 of the European Synchrotron Radiation Facility (ESRF). The X-ray beam was mono-chromatized with a Laue-Laue monochromator to the energy of 69 keV and focused to the size of $5 \times 20 \text{ µm}^2$ (vertical × horizontal) at the sample posi-

tion. The 2D XRD patterns were collected with a Dectris Pilatus 2M CdTe detector. A custom-made PEEK electrochemical flow cell was used for the experiments.[46] The measurements were performed in grazing incidence geometry (the incidence angle was less than 1 degree), in CO_2-sat. 0.5 M $KHCO_3$ electrolyte. A continuous flow of fresh CO_2-sat. electrolyte solution through the spectro-electrochemical cell prevented any undesired accumulation of soluble Cu species in the investigated X-ray window. All potentials were iR-corrected.

2.4 Operando Raman Spectroscopy[19]

Raman spectra were recorded using a LabRAM HR800 confocal microscope (Horiba Jobin Yvon) at a working distance of 8 mm between the objective lens (LMPLFLN from Olympus, 50X magnification) and the sample with a numerical aperture of 0.1 in order to focus a diode-pumped solid-state or He-NE laser beam (excitation wavelength of 532 or 633 nm, power of 3 mW) on the sample. The Raman signal was collected in a back-scattering geometry using a lab-made spectro-electrochemical cell made of Kel-F.[47,48] CO_2-sat. 0.5 M $KHCO_3$ solution was used as the electrolyte. The ohmic drop was determined using the positive feedback technique and compensated during the measurement.

2.5 Identical Location Scanning Electron Microscopy (IL-SEM)

For the high-resolution (HR) identical location (IL) SEM imaging a Zeiss DSM 982 instrument was used.

2.6 Product Analysis of the ec-CO2RR[11,18]

All electrolysis experiments were carried out in CO_2-sat. 0.5 M $KHCO_3$ solution using a custom-built, air-tight glass-cell (H-type) described elsewhere.[11] During electrolysis CO_2 was continuously purged through the catholyte at a flow rate of 13 mL × min⁻¹. The headspace of the electrolysis cell was directly connected to the gas sampling loop of the gas chromatograph (GC 8610C, SRI Instruments). The GC was equipped with a packed Haysep D column and a packed Molesieve 5A column. Argon (99.9999 %, Carbagas) was used as the carrier gas. A flame ionization detector (FID) coupled to a methanizer was used to quantify CO and volatile hydrocarbons. A thermal conductivity detector (TCD) was used for the H_2 detection. Non-volatile products (e.g. alcohols) were quantified by a second FID detector. After the electrolysis, a 2 µL aliquot of the electrolyte solution was injected into a second Haysep D column (post-electrolysis alcohol detection). Other liquid products (e.g. formate) were analyzed by means of ion exchange chromatography (IC, Metrohm Advanced Modular Ion Chromatograph: L-7100 pump, Metrosep A Supp 7-250 column, conductivity detector).

3. Results and Discussion

3.1 Activation of Cu Foam Electrocatalysts[19]

Fig. 5 displays a prime example of Cu foams fabricated by means of the DHBT-assisted electrodeposition method.[11] The basic concept of this approach was adapted from the work by Shin et al.[15,16] As the Cu electrodeposition takes place under rather harsh hydrogen evolution reaction (HER) conditions (e.g. at current densities of $j = -3$ A × cm⁻², see Fig. 4), gas bubbles rapidly evolve on the support electrode and serve as geometric template for the actual metal plating process which is superimposed on the HER. Cu is deposited only in the bubble-free areas of the support and the emerging porous film. The process of hydrogen bubble
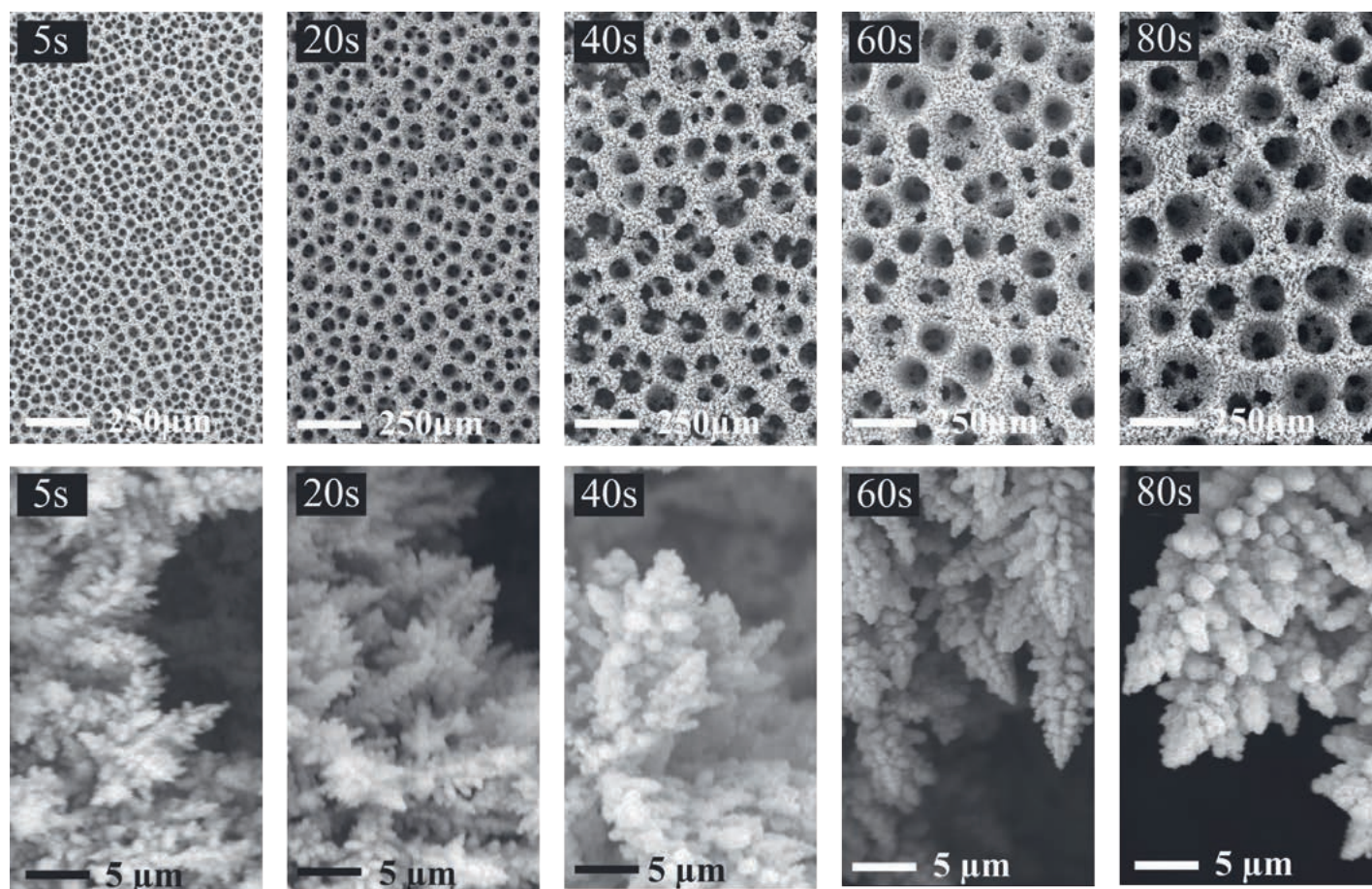

Fig. 5. Top-down SEM analysis showing the surface pore size (upper row) and dendrite size (lower row) evolution as function of the deposition time (exemplified for a Cu foam catalyst). Adapted from ref. [11], with permission of the American Chemical Society.

nucleation, growth and coalescence is continuous. This is why the average surface pore size increases as function of the deposition time and film thickness (Fig. 5).[11] A characteristic feature of the formed metal foams is a gradient in the pore sizes along the surface normal. Smallest pores are typically created close to the support electrode whereas the biggest ones are found at the outermost surface of the foam material which is exposed to the (liquid) electrolyte during the CO_2 electrolysis reaction.[11]

In addition to this primary macro-porosity (µm length scale), originated by the gaseous H_2-template during the metal deposition, the scaffold of the formed 3D foam itself is porous, too.[11,20,49] The macro-pore sidewalls are composed of randomly distributed Cu dendrites thus introducing a secondary porosity to the catalyst (nm length scale).[15] Such a dendritic growth mode originates from the applied experimental conditions that impose a deposition rate limited by mass transport of the metal ions and a reduced mobility of the deposited atoms on the emerging foam surface.[11]

In particular when alcohols are targeted as products, the electrodeposited catalysts often require further activation prior to the ec-CO_2RR, e.g. by thermal annealing in air.[28,50] Fig. 6 displays representative SEM micrographs of an 'as-deposited' Cu foam and its morphological evolution induced by thermal annealing at 300 °C for 12 h in air, and a subsequent 1 h CO_2 electrolysis in CO_2-sat. 0.5 M bicarbonate solution carried out at –0.67 V vs. RHE. Obviously, the macro-porous morphology of the Cu foam remains completely unaffected by both the thermal annealing in air (Cu oxidation) and the subsequent ec-CO_2RR, the latter involving the electro-reduction of the formed oxides.[19,20] However, the Cu foam undergoes substantial morphological alterations on the nm length scale particularly induced by the thermal treatment (see Fig. 6e–h). Following the 12 h annealing step at 300 °C, the surface of the pristine metallic Cu foam is completely transformed into a composite material consisting of cuprous (Cu_2O) and cupric (CuO) oxides[19,20,28] (denoted Cu_xO). This transformation requires substantial mass transport of oxygen and Cu species. A combination of ex situ (post-deposition, post-electrolysis) XRD and XPS analysis confirms the composite nature of the oxidic foam.[19,20] It should be noted that the applied annealing temperature of 300 °C is sufficient to form a crystalline Cu_2O phase whereas the cupric CuO remains largely in an amorphous state lacking any long range transitional order.[19,20] Consequently, Cu(II) species are detected in the XPS but not in the corresponding XRD analysis.[19,20] It should be noted here that, in full agreement with previous studies, the thermal annealing activates the Cu catalyst for C2 and C3 alcohol production.[19] For instance, the partial current density for ethanol formation increases from $j_{EtOH} = -0.86$ mA × cm⁻² ($FE_{EtOH} = 5\%$) at –0.77 V vs. RHE to $j_{EtOH} = -1.61$ mA × cm⁻² ($FE_{EtOH} = 6.7\%$) at –0.87 V vs. RHE. Similarly, the partial current density for n-propanol formation reaches a value of $j_{PrOH} = -1.72$ mA × cm⁻² ($FE_{PrOH} = 7.1\%$) at –0.87 V.[19] A full description of the electrocatalytic performance of the annealed Cu foam can be found in ref. [19].

More sophisticated operando analytical techniques are required to ultimately address how important oxide species are in particular for the alcohol electrosynthesis via the ec-CO_2RR on these Cu foams. Fig. 7 provides an overview on the results of the highly complementary XAS, XRD, and Raman spectroscopic investigations discussed by Dutta et al.[19] Changes in the potential-dependent Cu K-edge XANES spectra of the Cu_xO foam could be attributed to potential-dependent redox state changes of Cu species (Fig. 7, panel a; selected data set). Panel b in Fig.7 shows the result of a linear combination fitting (LCF) that was applied to the obtained XANES data using Cu K-edge XANES spectra of a Cu foil, Cu_2O and CuO as reference materials. The plot displays the relative concentrations of the Cu(0), Cu(I), and Cu(II) species present in the Cu_xO foam as a function of the potential applied.[19] The LCF analysis suggests that the Cu_xO foam at +0.6 V vs. RHE predominantly consists of CuO, whereas only a lower Cu_2O content was observed (25–35 wt.%). Upon potential excursion from +0.6 down to 0 V vs. RHE, the relative abundances of Cu(II) and Cu(I) anti-correlate and further negative polarization leads to the onset of oxide reduction to metallic Cu(0). At potentials below 0 V vs. RHE the Cu(II) abundance
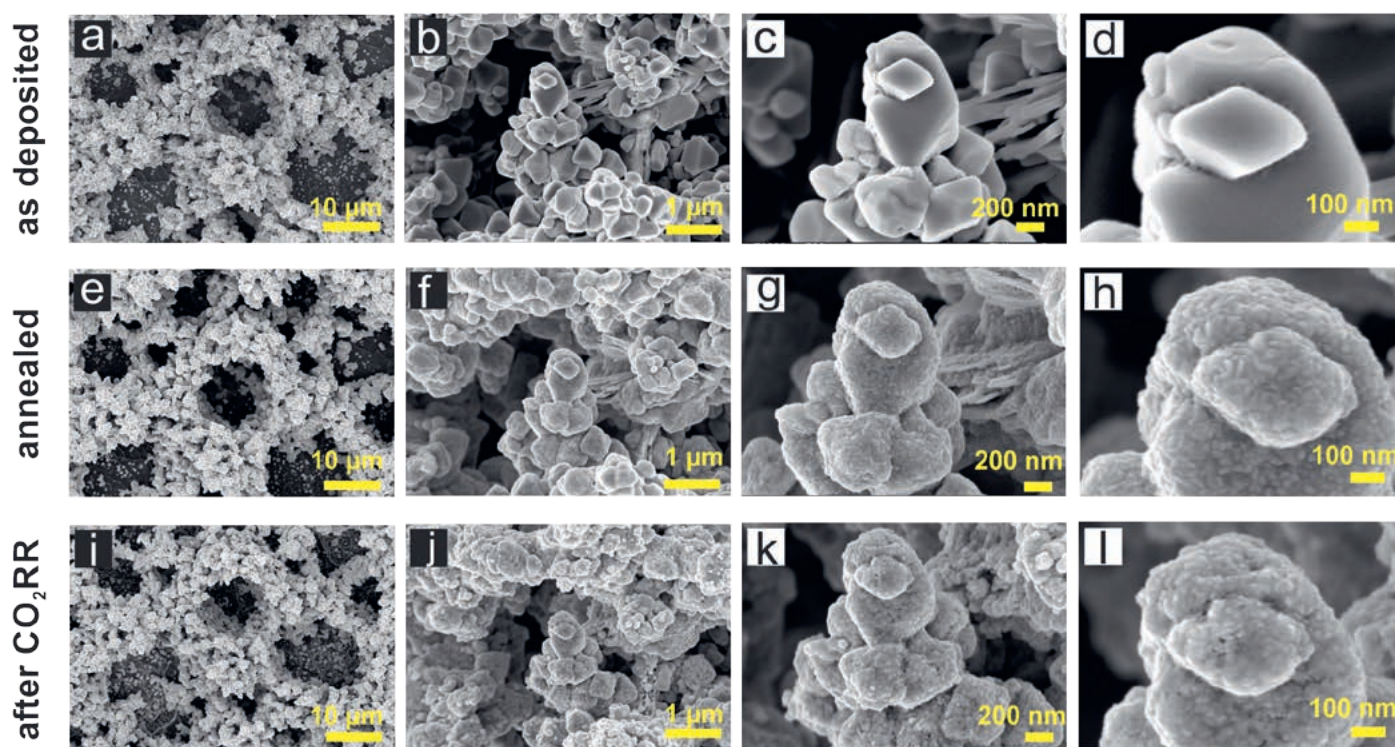

Fig. 6. Identical location (IL) SEM inspection of the Cu foam catalyst. (a–d) As-deposited Cu foam (5 s deposition at -3 A × cm⁻²); (e–h) Thermally annealed Cu foam (300 °C for 12 h in air, denoted Cu_xO foam); (i–l) Oxide-derived (OD) Cu foam after 1 h CO_2RR in CO_2-sat. 0.5 M KHCO₃ solution at –0.67 V vs. RHE. Adapted from ref. [19], with permission of Elsevier.
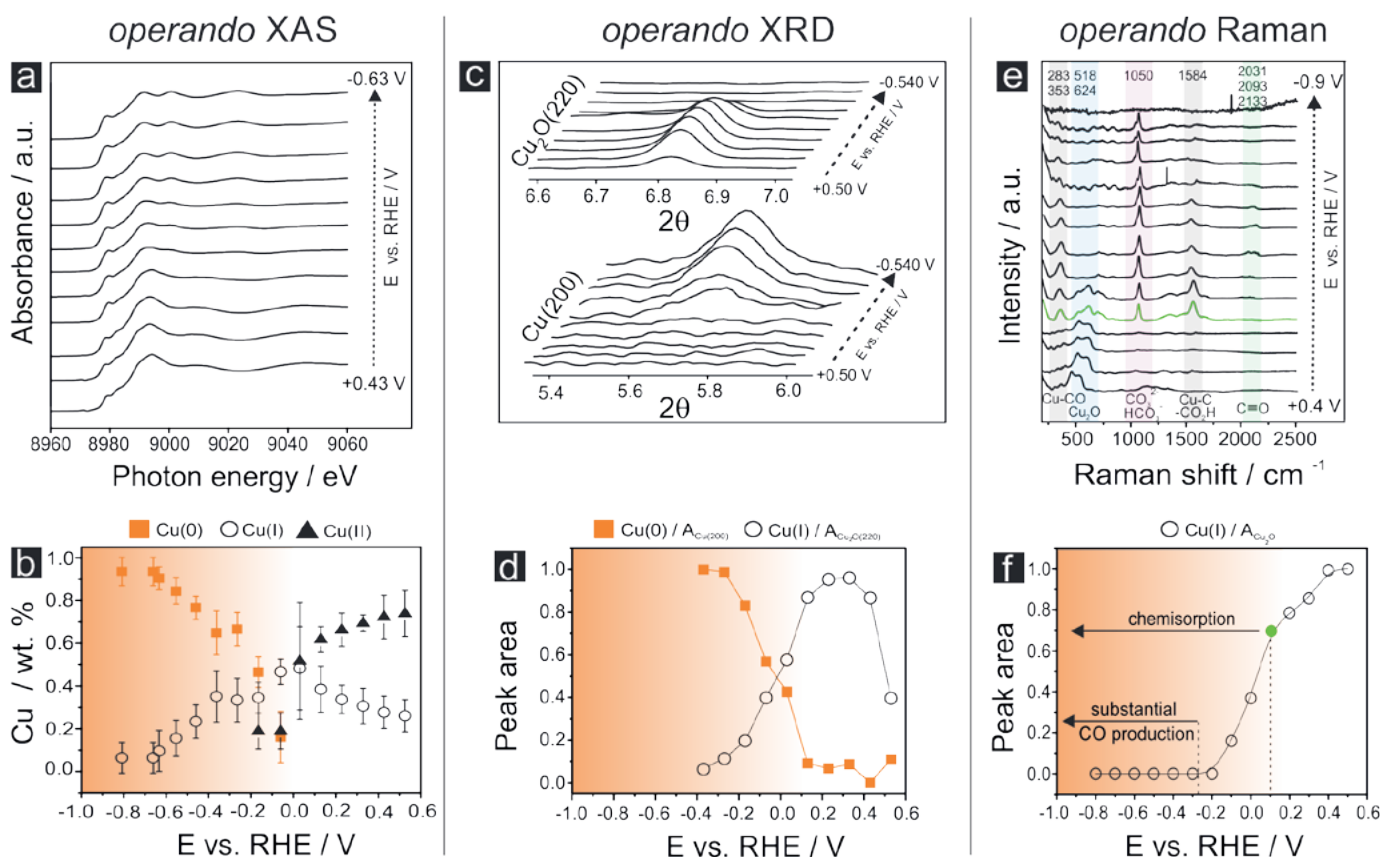
Fig. 7. Survey of experimental *operando* results demonstrating the potential-dependent oxide–metal transition of the oxidic catalyst precursor (Cu$_x$O foam). (a) Potential-dependent *operando* XANES spectra (Cu K-edge) of the thermally annealed Cu foam (Cu$_x$O) in CO$_2$-sat. 0.5 M KHCO$_3$ solution; (b) Potential-dependent composition of the Cu$_x$O foam (relative content of Cu species: Cu(0), Cu(I), and Cu(II) derived from a linear combination fitting (LCF) of the XANES spectra shown in (a)); (c) Potential-dependent *operando* grazing-incidence X-ray diffractograms of the Cu$_2$O(220) and Cu(200) reflections; (d) Integrated and normalized peak intensities of the diffractograms shown in (c); (e) Corresponding potential-dependent *operando* Raman spectra; (f) Integrated and normalized peak intensities of the Cu$_2$O-related Raman peaks (518 cm^{-1} and 624 cm^{-1}) shown in (e). The peak areas were normalized with respect to the most intense peaks at most positive electrode potentials. The grey and orange areas in panel b, d, and f indicate the stability windows of the oxidic and metallic state of Cu, respectively. Adapted from ref. [19], with permission of Elsevier.

drops down to zero, whereas Cu(I) species are present in the bulk material down to potentials of -0.5V vs. RHE.[19] The potential-dependent decrease of the Cu(I) content below 0 V vs. RHE is clearly anti-correlated to the increase of the Cu(0) abundance. The transition from the oxidic precursor to metallic Cu in the bulk is completed at about –0.7 V vs. RHE.[19]

Operando XRD experiments basically confirm the XAS investigations (panel c and d in Fig. 7). As hypothesized on the basis of the XAS results the integrated intensity of the Cu$_2$O(220) diffraction peak first increases when sweeping the cathode potential from +0.5 V to +0.2 V vs. RHE. This trend is consistent with the assumption of an intermediate crystalline Cu$_2$O phase which accumulates in the initial stage of the oxide–metal transition in the foam material at the expense of the amorphous CuO phase.[19] Interestingly, the disappearance of the Cu$_2$O related diffraction pattern with negative going potentials is already completed at –0.4 V vs. RHE, whereas the XAS experiment indicates the presence of Cu(I) species for potentials down to –0.8 V vs. RHE. These deviations in the particular potential-dependence of the Cu(I)(XAS)/Cu$_2$O(XRD) stability regime are related to the intrinsic characteristics of both *operando* techniques. The ultimate reduction of the Cu(I) to Cu(0) proceeds most likely *via* an intermediate amorphous Cu(I) phase.[19]

Among the *operando* techniques applied Raman spectroscopy is the most surface sensitive one.[19] Raman features observed at 148 cm^{-1}, 518 cm^{-1}, and 624 cm^{-1} can be ascribed to cuprous oxide species (Cu$_2$O), whereas vibrational modes at

298 cm^{-1} and 346 cm^{-1} originate from cupric oxides (panel e and f in Fig. 7).[19] Interesting to note is that after exposure to the 0.5 M KHCO$_3$ electrolyte at the open circuit potential, the CuO related vibrational modes have completely disappeared from the Raman spectra.[19] Only vibrational modes of the cuprous oxide (Cu$_2$O) are left which indicates that the initial catalyst surface is terminated exclusively by Cu(I) species when exposed to the electrolyte. Both XRD and XAS typically do not show these effects when the oxidic foam is exposed to the electrolyte at OCP.[19] This is due to the dominance of 'bulk' contributions to the data with only minor contributions from the foam surface. Integrated intensities of the Cu$_2$O specific Raman features (panel f) follow qualitatively the same trend as observed in the XAS and XRD. However, the 'surface oxide reduction' proceeds apparently faster than the corresponding transition of the oxidic 'bulk phases' probed by *operando* XAS and XRD and is therefore completed at less negative applied potentials.[19]

Operando Raman spectroscopy provides additional information on intermediate species associated to the ec-CO$_2$RR. Raman modes observed at 283 cm^{-1}/253 cm^{-1}, 1050 cm^{-1}, 1584 cm^{-1} and 2031 cm^{-1}/2093 cm^{-1}/2133 cm^{-1} are attributed to adsorbed CO, HCO$_3^-$, and HCOOH respectively. These intermediates appear only after partial reduction of the oxide to the metallic Cu.[19]

The 'holistic view' on the potential-dependent oxide–metal transition using different complementary *operando* techniques let us safely conclude that the surface and bulk Cu oxide reduction is completed at potentials more positive than the onset of hydrocar-

Fig. 8. (a,b) *ap* Bi/Bi$_x$O$_y$ foam deposited on a carbon cloth support (denoted Bi/Bi$_x$O$_y$@GDE); (c) CO$_2$RR product distribution represented as *FE*$_{formate}$ vs. E plot (*FE*: Faradaic efficiency). The annealed foam (denoted Bi$_2$O$_3$@GDE) was used as the catalyst; (d) Corresponding CO$_2$RR reaction rate represented as PCD$_{formate}$ vs. E plot (PCD: partial current density). Note that the only side-product of the CO$_2$RR is hydrogen; (e–h) *Operando* Raman spectroscopy results showing the potential-dependent oxide/sub-carbonate reduction. Raman bands at 313 cm^{-1} and 162 cm^{-1} were used to probe the presence of oxide and sub-carbonate species, respectively; (i) *Operando* optical inspection of the time-dependent oxide/sub-carbonate/metal transition in CO$_2$-sat. 0.5 M KHCO$_3$ solution at -0.6 V vs. RHE; (j,k) Proposed reaction mechanisms of formate formation. Adapted from ref. [18], with permission of the American Chemical Society.
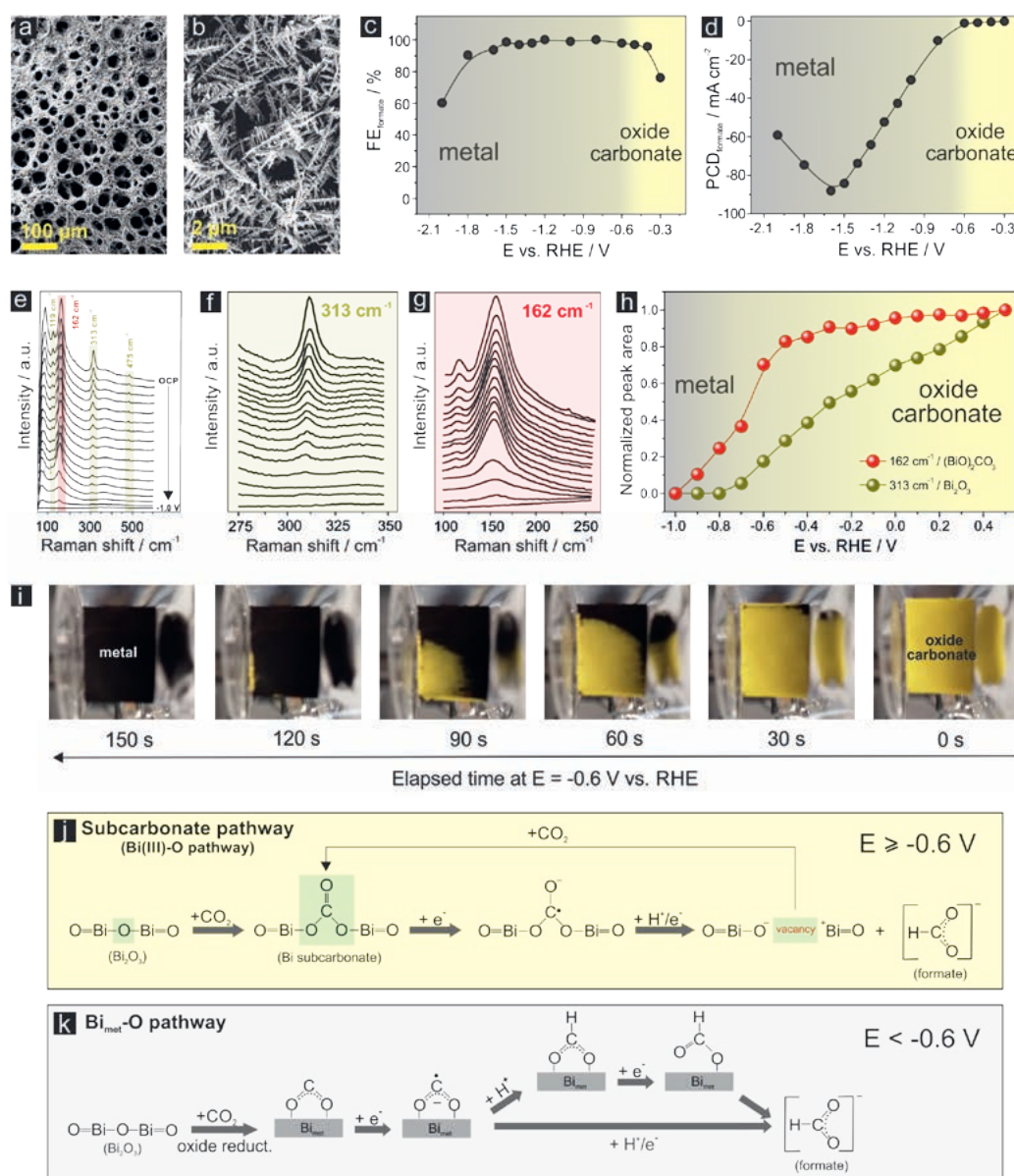
bon and alcohol formation. Obviously, oxidic species do not play any significant role for the ec-CO$_2$RR on Cu in general and for the alcohol production in particular.

3.2 *Activation of Bi/Bi$_2$O$_3$ Foam Electrocatalysts*[18]

A novel bismuth oxide (Bi$_2$O$_3$) foam-type of catalyst (precursor) material has been produced by means of an additive-assisted DHBT electrodeposition followed by thermal annealing at 300 °C for 12 h.[18] This DHBT approach could successfully be applied to functionalize technical supports, *e.g.* gas diffusion electrodes (GDEs). This transfer of the foam catalyst from planar substrates (*e.g.* Cu foils[11]) to highly porous carbon supports is considered a crucial technical pre-requisite for any future application of this novel catalyst concept in gas-fed (CO$_2$) electrolyzer systems. The latter will be vital to achieve ec-CO$_2$RR current densities which are of technological relevance ($j_{CO2RR} > 200$ mA × cm^{-2}). It should be noted that the resulting (surface) pore sizes are altered when changing the support material.[18] In general, the pore size distribution is substantially broader when the foam materials are electrodeposited on porous carbon supports compared to respective metal foaming processes on planar metal foil supports. Fig. 8a,b shows representative top-down SEM images of the as-prepared Bi foam on the technical carbon support denoted hereafter *ap* Bi/

Bi$_2$O$_3$@GDE. Note that the as-prepared oxophilic Bi foam is typically covered by an ultrathin Bi$_2$O$_3$ layer after its emersion from the Bi plating bath.[18]

The thermal treatment at 300 °C for 12 h in air leaves the macroporosity of *ap* Bi/Bi$_2$O$_3$ foam fully unaffected (see also Fig. 9), similar to the Cu case (Fig. 6). This annealing yields a fully oxidized Bi$_2$O$_3$ foam which shows a characteristic yellow color (Fig. 8i at 0 s).

The formed oxidic Bi foam exhibits a superior electrocatalytic selectivity toward formate production with Faradaic efficiencies (FEs) never falling below 90 % within an extraordinarily huge potential window of ~ 1100 mV (max. *FE*$_{formate}$ = 100% at –0.8 V vs. RHE).[18] Panel c and d of Fig. 8 depict the potential-dependent Faradaic efficiencies (c) and partial current densities (d) of formate production when the electrolysis is carried out from aqueous CO$_2$-sat. 0.5 M KHCO$_3$ solution.

For the first time, *operando* Raman spectroscopy provided clear experimental evidence for the embedment of CO$_2$ into an oxidic matrix (so-called 'sub-carbonate' formation) at low overpotentials prior to and during the CO$_2$ reduction reaction (Fig. 8e–h). We used the Raman bands at 313 cm^{-1} and 162 cm^{-1} as characteristic 'fingerprints' for the presence of Bi oxide and Bi subcarbonate species, respectively.[18] Note that
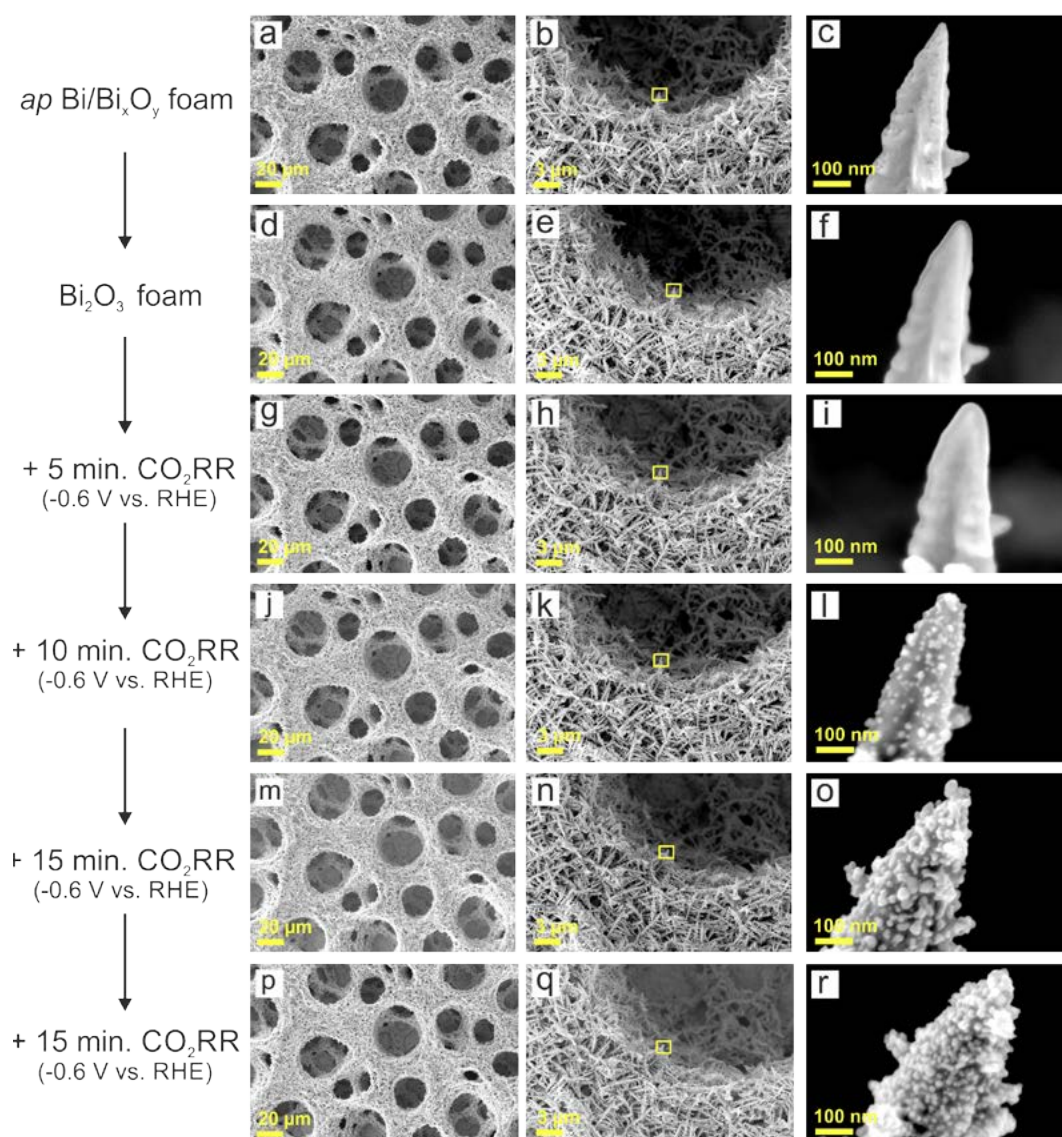
Fig. 9. (a-r) Identical location (IL) SEM inspection of morphological changes associated to the thermal annealing of the *ap* Bi/Bi$_x$O$_y$ foam, the sub-carbonate formation and subsequent potentiostatic CO$_2$ electrolysis in CO$_2$-sat. 0.5 M KHCO$_3$ solution at –0.6 V vs. RHE. Adapted from ref. [18] with permission of the American Chemical Society.

the exchange of the oxide by the sub-carbonate is a spontaneous and rather fast process which takes place in the CO$_2$-sat. 0.5 M KHCO$_3$ solution even at the open circuit potential without initiating the ec-CO$_2$RR. Indeed, the potential-dependent integrated intensities of the Raman bands at 313 cm^{-1} and 162 cm^{-1} suggest that formed sub-carbonate species are more stable than the corresponding oxides (Fig. 8h). As shown in Fig. 8i, this transition from the oxide/sub-carbonate to the metallic Bi state is accompanied by a characteristic color change from yellow (oxide) to black (metal).

These excellent electrocatalytic characteristics of the novel Bi foam catalysts result from the coupling of two distinct reaction pathways of formate formation which are active (i) in the presence of the (partly-reduced) Bi$_2$O$_3$ foam at low overpotentials (sub-carbonate pathway) and (ii) on the corresponding metallic Bi foam catalyst at medium and high overpotentials (Bi-O pathway). The reaction mechanisms, proposed also on the basis of the *operando* Raman results, are displayed in Fig. 8j,k. To probe in more detail the structural and morphological changes which take place on the nanometer length scale upon sub-carbonate formation and partial electro-reduction of the oxidic precursor during ec-CO$_2$RR we further applied the identical location (IL) scanning electron microscopy (SEM) technique

by sequentially imaging the same single spot on the catalyst surface after the initial electrodeposition (as prepared), after the thermal annealing treatment, and after a series of dedicated CO$_2$ electrolyses. The results of this IL-SEM analysis are depicted in Fig. 9 and demonstrate severe morphological changes on the nm length scale which go along with (i) the oxidation upon thermal annealing, (ii) the sub-carbonate formation when exposed to the CO$_2$-sat. bicarbonate solution, and (iii) the ensuing catalyst electro-reduction into the metallic state at higher applied overpotentials.

These microscopic results impressively demonstrate that the actually active catalyst forms only under reactive conditions.

4. Conclusions

Herein we have demonstrated the usefulness of advanced *operando* analytical techniques to probe the (chemical) state evolution of foam-type catalysts under reactive conditions, *e.g.* in the course of CO$_2$ electrolysis. In particular for the case of Cu foams and their oxidic precursors it could be shown that a complementary *operando* analysis approach is mandatory to derive a full understanding of the catalyst activation process which involves the potential-driven electro-reduction of the oxidic precursors. Due to intrinsic technical limitations associated with

each applied *operando* technique (*e.g.* XAS, XRD, and Raman spectroscopy) the probed potential dependence of the observed structural and compositional alterations is slightly different in all cases. However, from all applied *operando* techniques it can be concluded that the oxide–metal transition is completed prior to the onset of hydrocarbon or alcohol formation. The active Cu catalyst can be indeed considered as metallic (oxide-derived).

The understanding of the catalyst activation process is, however, much more complex in case of Bi foams and their oxidic counterparts. As evidenced by the comparison of *operando* Raman spectroscopy results and corresponding electrochemical performance testing, both the oxidic and the metallic foams are active towards ec-CO$_2$RR (formate production). The scenario becomes even more complex due to the rapid exchange of oxidic species by sub-carbonates in the presence of (dissolved) CO$_2$ in the electrolyte solution. It is the coupling of two distinct reaction pathways of formate production (sub-carbonate pathway at low overpotentials; Bi-O pathway at high overpotentials) that leads to the extraordinarily broad potential window of ~1100 mV in which the Faradaic efficiency of formate production does not fall below 90%.

Acknowledgments

Received: July 1, 2021

[1] E. V. Kondratenko, G. Mul, J. Baltrusaitis, G. O. Larrazabal, J. Perez-Ramirez, *Energy Environ. Sci.* **2013**, *6*, 3112, https://doi.org/10.1039/C3EE41272E

[2] M. Fasihi, O. Efimova, C. Breyer, *J. Clean. Prod.* **2019**, *224*, 957, https://doi.org/10.1016/j.jclepro.2019.03.086

[3] S. Fujikawa, R. Selyanchyn, T. Kunitake, *Polym. J.* **2021**, *53*, 111, https://doi.org/10.1038/s41428-020-00429-z

[4] N. McQueen, K. V. Gomes, C. McCormick, K. Blumanthal, M. Pisciotta, J. Wilcox, *Prog. Energy* **2021**, *3*, 032001, https://doi.org/10.1088/2516-1083/abf1ce

[5] T. Haas, R. Krause, R. Weber, M. Demler, G. Schmid, *Nat. Catal.* **2018**, *1*, 32, https://doi.org/10.1038/s41929-017-0005-1

[6] N. Kittner, F. Lill, D. M. Kammen, *Nat. Energy* **2017**, *2*, 17125, https://doi.org/10.1038/nenergy.2017.125

[7] B. D. Solomon, K. Krishna, *Energy Policy* **2011**, *39*, 7422, https://doi.org/10.1016/j.enpol.2011.09.009

[8] A. V. Rudnev, Y.-C. Fu, I. Gjuroski, F. Stricker, J. Furrer, N. Kovács, S. Vesztergom, P. Broekmann, *ChemPhysChem* **2017**, *18*, 3153, https://doi.org/10.1002/cphc.201700737

[9] J. Durst, A. Rudnev, A. Dutta, Y. Fu, J. Herranz, V. Kaliginedi, A. A. Permyakova, Y. Paratcha, P. Broekmann, T. J. Schmidt, *Chimia* **2015**, *69*, 769, https://doi.org/10.2533/chimia.2015.769

[10] Y. Hori, in 'Modern Aspects of Electrochemistry', Springer, New York, **2008**, 89, https://doi.org/10.1007/978-0-387-49489-0_3.

[11] A. Dutta, M. Rahaman, N. C. Luedi, M. Mohos, P. Broekmann, *ACS Catal.* **2016**, *6*, 3804, https://doi.org/10.1021/acscatal.6b00770

[12] J. Quinson, S. Neumann, T. Wannmacher, L. Kacenauskaite, M. Inaba, J. Bucher, F. Bizzotto, S. B. Simonsen, L. T. Kuhn, D. Bujak, A. Zana, M. Arenz, S. Kunz, *Angew. Chem. Int. Ed.* **2018**, *57*, 12338, https://doi.org/10.1002/anie.201807450

[13] M. de Jesus Gálvez-Vázquez, P. Moreno-García, H. Xu, Y. Hou, H. Hu, I. Z. Montiel, A. V. Rudnev, S. Alinejad, V. Grozovski, B. J. Wiley, M. Arenz, P. Broekmann, *ACS Catal.* **2020**, *10*, 13096, https://doi.org/10.1021/acscatal.0c03609

[14] M. d. J. Gálvez-Vázquez, S. Alinejad, H. Hu, Y. Hou, P. Moreno-García, A. Zana, G. K. H. Wiberg, P. Broekmann, M. Arenz, *Chimia* **2019**, *73*, 922, https://doi.org/10.2533/chimia.2019.922

[15] H. C. Shin, M. Liu, *Chem. Mater.* **2004**, *16*, 5460, https://doi.org/10.1021/cm048887b

[16] H. C. Shin, J. Dong, M. Liu, *Adv. Mater.* **2004**, *16*, 237, https://doi.org/10.1002/adma.200305660

[17] S. Vesztergom, A. Dutta, M. Rahaman, K. Kiran, I. Zelocualtecatl Montiel, P. Broekmann, *ChemCatChem* **2021**, *13*, 1039, https://doi.org/10.1002/cctc.202001145

[18] A. Dutta, I. Zelocualtecatl Montiel, K. Kiran, A. Rieder, V. Grozovski, L. Gut, P. Broekmann, *ACS Catal.* **2021**, *11*, 4988, https://doi.org/10.1021/acscatal.0c05317

[19] A. Dutta, M. Rahaman, B. Hecker, J. Drnec, K. Kiran, I. Zelocualtecatl Montiel, D. Jochen Weber, A. Zanetti, A. Cedeño López, I. Martens, P. Broekmann, M. Oezaslan, *J. Catal.* **2020**, *389*, 592, https://doi.org/10.1016/j.jcat.2020.06.024

[20] A. Dutta, M. Rahaman, M. Mohos, A. Zanetti, P. Broekmann, *ACS Catal.* **2017**, *7*, 5431, https://doi.org/10.1021/acscatal.7b01548

[21] M. G. Kibria, C.-T. Dinh, A. Seifitokaldani, P. De Luna, T. Burdyny, R. Quintero-Bermudez, M. B. Ross, O. S. Bushuyev, F. P. García de Arquer, P. Yang, D. Sinton, E. H. Sargent, *Adv. Mater.* **2018**, *30*, 1804867, https://doi.org/10.1002/adma.201804867

[22] Y. Hori, A. Murata, R. Takahashi, *J. Chem. Soc., Faraday Trans. 1* **1989**, *85*, 2309, https://doi.org/10.1039/F19898502309

[23] Y. Hori, I. Takahashi, O. Koga, N. Hoshi, *J. Phys. Chem. B* **2002**, *106*, 15, https://doi.org/10.1021/jp013478d

[24] S. Ma, M. Sadakiyo, R. Luo, M. Heima, M. Yamauchi, P. J. A. Kenis, *J. Power Sources* **2016**, *301*, 219, https://doi.org/10.1016/j.jpowsour.2015.09.124

[25] J. J. Kim, D. P. Summers, K. W. Frese, *J. Electroanal. Chem.* **1988**, *245*, 223, https://doi.org/10.1016/0022-0728(88)80071-8

[26] K. P. Kuhl, T. Hatsukade, E. R. Cave, D. N. Abram, J. Kibsgaard, T. F. Jaramillo, *J. Am. Chem. Soc.* **2014**, *136*, 14107, https://doi.org/10.1021/ja505791r

[27] M. Rahaman, K. Kiran, I. Z. Montiel, V. Grozovski, A. Dutta, P. Broekmann, *Green Chem.* **2020**, *22*, 6497, https://doi.org/10.1039/D0GC01636E

[28] M. Rahaman, A. Dutta, A. Zanetti, P. Broekmann, *ACS Catal.* **2017**, *7*, 7946, https://doi.org/10.1021/acscatal.7b02234

[29] R. Kas, R. Kortlever, A. Milbrat, M. T. M. Koper, G. Mul, J. Baltrusaitis, *Phys. Chem. Chem. Phys.* **2014**, *16*, 12194, https://doi.org/10.1039/C4CP01520G

[30] C. W. Li, J. Ciston, M. W. Kanan, *Nature* **2014**, *508*, 504, https://doi.org/10.1038/nature13249

[31] K. W. Frese, *J. Electrochem. Soc.* **1991**, *138*, 3338, https://doi.org/10.1149/1.2085411

[32] M. Ma, K. Djanashvili, W. A. Smith, *Phys. Chem. Chem. Phys.* **2015**, *17*, 20861, https://doi.org/10.1039/C5CP03559G

[33] D. Gao, I. Zegkinoglou, N. J. Divins, F. Scholten, I. Sinev, P. Grosse, B. Roldan Cuenya, *ACS Nano* **2017**, *11*, 4825, https://doi.org/10.1021/acsnano.7b01257

[34] C. W. Li, M. W. Kanan, *J. Am. Chem. Soc.* **2012**, *134*, 7231, https://doi.org/10.1021/ja3010978

[35] B. Beverskog, I. Puigdomenech, *J. Electrochem. Soc.* **1997**, *144*, 3476, https://doi.org/10.1149/1.1838036

[36] A. Verdaguer-Casadevall, C. W. Li, T. P. Johansson, S. B. Scott, J. T. McKeown, M. Kumar, I. E. L. Stephens, M. W. Kanan, I. Chorkendorff, *J. Am. Chem. Soc.* **2015**, *137*, 9808, https://doi.org/10.1021/jacs.5b06227

[37] H. Mistry, A. S. Varela, C. S. Bonifacio, I. Zegkinoglou, I. Sinev, Y. W. Choi, K. Kisslinger, E. A. Stach, J. C. Yang, P. Strasser, B. R. Cuenya, *Nat. Commun.* **2016**, *7*, https://doi.org/10.1038/ncomms12123

[38] A. Eilert, F. Cavalca, F. S. Roberts, J. Osterwalder, C. Liu, M. Favaro, E. J. Crumlin, H. Ogasawara, D. Friebel, L. G. M. Pettersson, A. Nilsson, *J. Phys. Chem. Lett.* **2017**, *8*, 285, https://doi.org/10.1021/acs.jpclett.6b02273

[39] F. Cavalca, R. Ferragut, S. Aghion, A. Eilert, O. Diaz-Morales, C. Liu, A. L. Koh, T. W. Hansen, L. G. M. Pettersson, A. Nilsson, *J. Phys. Chem. C* **2017**, *121*, 25003, https://doi.org/10.1021/acs.jpcc.7b08278

[40] M. Fields, X. Hong, J. K. Nørskov, K. Chan, *J. Phys. Chem. C* **2018**, *122*, 16209, https://doi.org/10.1021/acs.jpcc.8b04983

[41] A. J. Garza, A. T. Bell, M. Head-Gordon, *J. Phys. Chem. Lett.* **2018**, *9*, 601, https://doi.org/10.1021/acs.jpclett.7b03180

[42] P. Grosse, D. Gao, F. Scholten, I. Sinev, H. Mistry, B. Roldan Cuenya, *Angew. Chem. Int. Ed.* **2018**, *57*, 6192, https://doi.org/10.1002/anie.201802083

[43] K. J. J. Mayrhofer, S. J. Ashton, J. C. Meier, G. K. H. Wiberg, M. Hanzlik, M. Arenz, *J. Power Sources* **2008**, *185*, 734, https://doi.org/10.1016/j.jpowsour.2008.08.003

[44] T. Kottakkat, K. Klingan, S. Jiang, Z. P. Jovanov, V. H. Davies, G. A. M. El-Nagar, H. Dau, C. Roth, *ACS Appl. Mater. Interfaces* **2019**, *11*, 14734, https://doi.org/10.1021/acsami.8b22071

[45] M. R. Antonio, L. Soderholm, I. Song, *J. Appl. Electrochem.* **1997**, *27*, 784, https://doi.org/10.1023/A:1018464526864

[46] I. Martens, R. Chattot, M. Rasola, M. V. Blanco, V. Honkimäki, D. Bizzotto, D. P. Wilkinson, J. Drnec, *ACS Appl. Energy Mater.* **2019**, *2*, 7772, https://doi.org/10.1021/acsaem.9b00982

[47] A. Dutta, A. Kuzume, M. Rahaman, S. Vesztergom, P. Broekmann, *ACS Catal.* **2015**, *5*, 7498, https://doi.org/10.1021/acscatal.5b02322

[48] A. Dutta, A. Kuzume, V. Kaliginedi, M. Rahaman, I. Sinev, M. Ahmadi, B. R. Cuenya, S. Vesztergom, P. Broekmann, *Nano energy* **2018**, *53*, 828, https://doi.org/10.1016/j.nanoen.2018.09.033
[49] A. Dutta, C. E. Morstein, M. Rahaman, A. Cedeño López, P. Broekmann, *ACS Catal.* **2018**, *8*, 8357, https://doi.org/10.1021/acscatal.8b01738
[50] A. Dutta, I. Z. Montiel, R. Erni, K. Kiran, M. Rahaman, J. Drnec, P. Broekmann, *Nano Energy* **2020**, *68*, 104331, https://doi.org/10.1016/j.nanoen.2019.104331